Soft Matter

Accepted Manuscript

ROYAL SOCIETY OF CHEMISTRY

www.rsc.org/softmatter

The combination of mold casting and aligned nanofibers with chondroitin sulfate, hyaluronic acid, and polycaprolactone is used to create scaffolds for the regeneration of osteochondral tissue. When seeded with bone marrow stromal cells, the scaffolds were able to initiate chondrogenesis and osteogenesis. This study shows that when co-cultured together there is potential for the formation of bone and cartilage tissue.

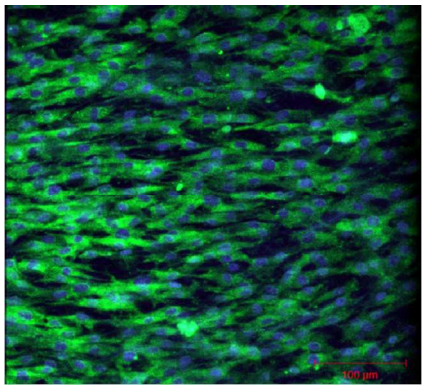

Soft Matter

ARTICLE

Guided Differentiation of Bone Marrow Stromal Cells on Co-Cultured Cartilage and Bone Scaffolds

Paul Lee[a], Katelyn Tran[a], Gan Zhou[a], Asheesh Bedi[b], Namdev B. Shelke[c], Xiaojun Yu*[a] and Sangamesh G. Kumbar*[c]

Received 00th January 20xx,
Accepted 00th January 20xx

DOI: 10.1039/x0xx00000x

www.rsc.org/

Focal chondral defects that result from traumatic injuries to the knee remain one of the most common causes of disability in patients. Current solutions for healing focal cartilage defects are mainly limited by the production of inferior cartilage-like tissue and subsequent delamination due to incomplete healing of the subchondral bone. In this experiment a polymeric osteochondral implant for guiding autologous bone marrow stem cells (BMSCs) to populate the scaffold to create distinctive bone and cartilage tissue. The cartilage component present bioactive aligned nanofibers containing chondroitin sulfate and hyaluronic acid while the bone component includes hydroxyapatite to promote chondrogenic and osteogenic differentiation of the rat BMSCs *in vitro*. The different cartilage and bone components resulted in the elevated expression of osteogenic markers such as bone sialoprotein, runt related transcription factor 2, and bone morphogenetic protein 2 in the deeper bone layer and chondrogenic markers such as collagen type II and aggrecan in the cartilage layer. Through immunofluorescence imaging, the alignment of the secreted collagen type II fibrils and aggrecan was visualized and quantified on the cartilage component of the scaffold. These current studies show that the biodegradable biphasic osteochondral implant may be effective in promoting more hyaline-like tissue to fill in chondral defects of the knee.

1. Introduction

One of the most debilitating diseases is osteoarthritis (OA), which carries an annual burden of $65 billion in 2001 to the United States health system alone. [1] The etiology of OA is multifactorial, but usually progresses from generalized overload or focal, traumatic chondral defects. [1] In many cases, early OA is brought on by traumatic injury to the joints secondary to contact or noncontact pivoting injuries.

The commonly available current treatments of the focal chondral defect include cell-based technologies, whole tissue transplantation of autograft or allograft, and marrow stimulation/microfracture. Autologous chondrocyte implantation (ACI) is one cell-based approach that has offered some promise. However, this treatment has only a 5 year improvement in condition rate of 71% and even longer term questionable durability. [2-4] Autograft transplantation has the best potential to achieve hyaline cartilage within the defect, but the limited availability and donor site morbidity is an significant concern. Microfracture utilizes penetrating holes in the subchondral bone to release bone marrow stem cells (BMSCs) to populate the defect with cells that may differentiate into chondrocytes. Unfortunately, the technique usually promotes the formation of fibrocartilage (mainly type I collagen, instead of type II), which lacks the functionality and durability of hyaline cartilage. [5] Even if chondrogenesis and collagen type II production occurs, it does not guarantee that functionally organized tissue will be created with native architecture or that complete fill of the defect will be achieved. [2, 6-10] One of the major reasons for the formation of fibrocartilage is the lack of attachment sites and chondrogenic materials for the cells, thus resulting in cell death and lack of differentiation. [11-13] One of the main characteristics of articular cartilage is its ability to resist shear and compressive stresses exerted between the joints during ambulation. This resistance to mechanical stresses is due to the unique alignment of collagen type II fibrils in tension [14]. The perpendicular alignment of the fibrils in the bottom layers of cartilage assist in the resistance to compressive stresses, this layer is 30-50% of the total thickness of total articular cartilage. [15] Another reason for failure is the potential for delamination of the tissue due to incomplete integration with the subchondral bone. [16] To prevent delamination of tissue, biphasic osteochondral implants are used to simultaneously regenerate bone and cartilage to increase integration. [17]

In order to overcome these challenges, we have developed a novel osteochondral scaffold that is capable of regenerating

[a] *Department of Chemistry, Chemical Biology and Biomedical Engineering, Stevens Institute of Technology, Hoboken, USA.* E-mail: xyu@stevens.edu; Fax: + *201)216-5256*; Tel: +*(201)216-8309*
[b] *University of Michigan Health System: MedSport, Lobby A, Domino's Farms, 24 Frank Lloyd Wright Drive, Ann Arbor, Michigan 481052, USA.*
[c] *Departments of Orthopaedic Surgery, Biomedical Engineering and Materials Science and Engineering, University of Connecticut, Farmington/Storrs, USA.* E-mail: Kumbar@uchc.edu; Fax: +(860) 679-1553; Tel: +(860) 679-3955.
† Footnotes relating to the title and/or authors should appear here.
Electronic Supplementary Information (ESI) available: [details of any supplementary information available should be included here]. See DOI: 10.1039/x0xx00000x

the underlying subchondral bone, while promoting the formation of cartilage that is morphologically similar and organized like articular cartilage. While the osteochondral model has been implemented in many designs, the key feature of the scaffold is the capability to potentially mimic the hyaline cartilage architecture using aligned nanofibers (Figure 1A). The scaffold consists of two spiral, nanofiber laden porous scaffolds fused together that can regenerate bone and cartilage in their respective areas. Nanofibers have been commonly used in many biomimetic applications, in this scaffold they can help recreate the extracellular matrix (ECM) that is native to hyaline cartilage, while increasing cellular attachment. The porosity of the scaffold of 106 to 150 µm allows for optimal cell migration, waste and nutrient transfer, while using sodium chloride as a porogen. [17] The spiral structure allows for higher surface area for nanofiber exposure due to the need for a flat open surface for the electrospinning of the fibers. [18, 19]

The spiral shape of the scaffold allows for flow of cells, nutrients, and waste through the construct. With the use of aligned polymeric poly-caprolactone (PCL) nanofibers combined with naturally occurring materials such as chondroitin sulfate (CS), hyaluronic acid (HYA), and hydroxyapatite (HA), we hypothesized that there is differentiation of both types of tissues with the two nanofibers scaffolds along with the alignment of the collagen type II fibrils in the cartilage region. [20-22] Biodegradable polyester PCL is commonly used in many biomedical applications has good biodegradability, processibility, and it does not degrade into acidic byproducts thus avoiding any inflammatory response, unlike some other polyesters. The other major structural extracellular matrix (ECM) components of cartilage CS and HYA both are glycosaminoglycans (GAGs). These GAGs are known to increase resistance to compressive stresses and HYA contributes to promoting ECM secretion, cell proliferation, migration, and helping to maintain chondrocyte phenotype and genotype, respectively. HA has been shown to increase osteoblast function, growth, and differentiation. With the use of differentiated zones of CS and HYA in the cartilage layer and HA in the bone layer, cartilage and bone growth should be

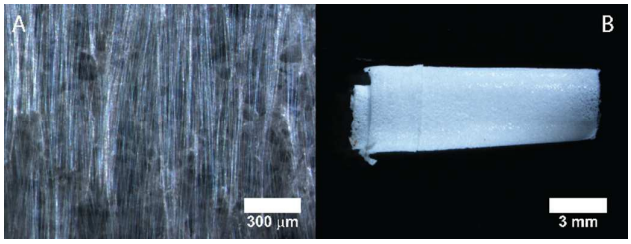

Fig. 1 – (A) Optical micrographs of the aligned inner nanofibers at 10X and (B) of the lateral view of the entire osteochondral scaffold at with the cartilage side on the left and the bone on the left 0.75X

localized to their respective zones when seeded with BMSCs without the use of growth factors such as transforming growth factors (TGFs) or bone morphogenetic proteins (BMPs). With the design of the scaffold, the bone side can be osteointegrative to anchor the cartilage zone and prevent delamination.

Through characterization of increased gene expression and immunofluorescence staining for bone and chondrogenic markers, we hypothesize that individual spiral bone and cartilage scaffolds are able initiate differentiation of rat BMSCs into bone and cartilage tissues respectively under the same *in vitro* culture conditions. [17, 21-25] In the cartilage region, chondrogenesis should be associated with increased gene expression in Aggrecan, Sox-9, and collagen type II**.** In the bone region, there should be an increased gene expression in collagen type I, Osteopontin (OPN), bone sialoprotein (BSP), bone morphogenetic protein 2 (BMP-2). Additionally, due to the use of known non cytotoxic materials, there should be an increase in cellular viability seen throughout the 28 day culture period in culture medium without any additional growth factors. With the use of BMSCs, comparisons can be made against microfracture technique simulating acellular implantation in the knee as a single stage procedure.

2. Materials and Methods

2.1 Scaffold Construction

Pilot experiments determined the effects of the two separate cartilage and bone layers cultured together with rat primary BMSCs under the same culture condition. For both cartilage and bone regeneration scaffolds, a porous PCL sheet laden with PCL nanofibers was used. Each scaffold contained different factors; for the cartilage scaffold, CS and HYA were imbedded into the nanofibers and for the bone scaffold, HA was embedded into the PCL sheet as well as the nanofibers themselves.

PCL (MW: 70,000 – 90,000), CS A from bovine trachea, HYA sodium salt from Streptococcus equi, and HA came from Sigma Aldrich (St. Louis, MO). Sodium Chloride (NaCl) was bought from Fisher Scientific (Pittsburgh, PA). 1,1,1,3,3,3 Hexafluoro-2-propanol (HFIP) was obtained from Oakwood Products, while dichloromethylene (DCM) came from (Pharmco-AAPER, Brookfield, CT).

The porous PCL sheets were made using the same technique from our previous experiments using mold casting by dissolving PCL in DCM at a 6% (w/v) concentration. [23, 26-28] To create pores, 106 to 150 µm salt particles were laden on a glass petri dish made sticky with a glucose solution for a uniform layer of porogen, where the PCL solution was poured into the dish. Once the DCM was evaporated, the salt was dissolved with DI water overnight to ensure proper pore formation. For the bone scaffold 20% HA (w/w) was added into the PCL solution before casting. The cartilage scaffolds were cut into 50 mm by 3 mm height strips, while the bone scaffolds were cut into 50 mm by 9 mm height strips. For the bone scaffold, 20% HA (w/w) was added into the solution before being casted. This size was chosen as the thickness most matches that of the cartilage and average subchondral bone thickness.

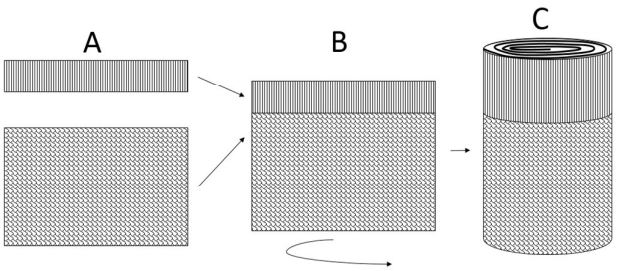

Fig. 2 – The process of fabricating the osteochondral scaffold where (A) uni-axially aligned nanofibers with CS and HYA constitute the upper cartilage part, while the lower randomly oriented nanofibers with HA bone region. (B) Edges of the two scaffold components were fused together with an aid of a metal block at 80 °C. (C) The fused matrix is rolled up into a spiral structure with the aid of copper sheet and heated at 45 °C for 1 hour. The copper sheet was pulled off to get the polymeric spiral structures.

Nanofiber solutions were prepared by dissolving PCL in an 8% (w/v) solution. Once fully dissolved, CS and HYA or HA were added to the mixture depending on whether it was a cartilage or bone scaffold, respectively. For the cartilage scaffold, 20% CS and 1% HYA (w/w) was added into the solution where DiH2O was added to form a 10% (v/v) solution to help dissolve the CS and HYA. For the bone scaffold, 20% (w/w) HA was added into the PCL nanofiber solution. Once completely dissolved, the solutions were loaded into 5 ml syringes with a 20G blunt tip needle (BD, Franklin Lakes, NJ). For bone and cartilage scaffolds, the nanofibers were electrospun using a 12 kV potential, with the substrate at a distance of 10 cm from the end of the needle, at a rate of 0.4 ml/hr for 4 minutes. To create the aligned fibers, the cartilage scaffolds were placed on a glass slide which was placed on grounded metal blocks under the electrospinner setup. The glass slides allows for vertical fiber formation by conducting only on the metal blocks. By aligning the PCL scaffold lengthwise between the metal blocks, it allowed nanofibers to be aligned perpendicularly with length of the scaffold during electrospinning (Figure 1A). The biphasic scaffold is presented in Figure 1B.

For the bone scaffold, the nanofibers were spun randomly by placing the PCL/HA scaffolds directly on a grounded foil surface underneath the needle at the same distance of 10 cm.

To immobilize the CS and HYA, the PCL in the cartilage scaffold was first functionalized with 5% (w/v) 1,6 hexanediamine in 95% isopropyl alcohol for 1 hour at 37 °C, then triple washed with phosphate buffered saline (PBS). Crosslinking was then performed using the EDC/NHS carbodiimide mechanism with 48 mM EDC, 6 mM NHS, and 50 mM MES buffer in water by immersing the functionalized cartilage scaffold for 24 hours at 37°C. Two scaffold components were fabricated separately as presented in figure 2. The edges of two scaffold components were fused by heating with the aid of metal block heated at 80°C, above the meting temperature of the polymer. The fused polymeric sheet was laid on a thin copper sheet and rolled into a spiral structure. The entire assembly was heated in an oven at 45°C for 1h. Upon cooling to room temperature the copper sheet was pulled off to retain the polymeric biphasic scaffold (Figure 1B and 2 C). Both bone and cartilage scaffolds were then rolled into spiral scaffolds lengthwise and bound with a copper strip and then heated to 45 °C for 1 hour to retain the shape. Thus the cartilage scaffold aligned nanofibers were aligned uniaxial to the spiral. The scaffolds were then triple washed with DI water and sterilized with 70% isopropyl alcohol and then triple washed with PBS.

2.2 Pull- out Testing

To determine the bonding strength between two scaffold components and access scaffold survivability within the implant space pull out tests were performed. The retention strength was determined at a ramp speed of 1.3 mm/sec using a 20 N load cell (Instron®), where an N # of 4 was used.

2.3 BMSC Culture and Seeding

Frozen Rat BMSCs were cultured until the second to third passage in AMEM with 10% FBS and 1% Penicillin (v/v). Once confluent, the cells were trypsinized and seeded at $5x10^4$ cells per cartilage and bone scaffold. The cartilage and bone scaffold were kept in the same well with each other, incubated at 37°C in DMEM with 10% (v/v) FBS, 1% (v/v) penicillin, and 0.03% HYA (w/v) to simulate a 5% synovial fluid environment. [29] $5x10^4$ cells were seeded into wells of a 24 well plate as a tissue culture plate (TCP) control. The medium was changed every other day.

2.4 Proliferation and Gene Expression

Table 1. List of primers used for RT-PCR

	Forward	Reverse	Amplicon Length	Accession #
GAPDH	GTCTACTGGCGTCTTCACC	AGGGATGATGTTCTGGGCTG	334	NM_017008.4
Aggrecan	AACTTCTTCGGAGTGGGTGG	CTGCTGTGCCTCCTCAAATG	444	NM_022190.1
ALP	TCCATGGTGGATTATGCTCA	TTCTGTTCCTGCTCGAGGTT	398	NM_013059.1
Collagen type I	TGTTCGTGGTTCTCAGGGTAG	TTGTCGTAGCAGGGTTCTTTC	280	NM_053356.1
Collagen type II	CTGCTCCTAGAGCCTCCTGC	GCCCTAATTTTCGGGCATCC	211	NM_012929.1
BMP-2	GAAGCCAGGTGTCTCCAAGAG	GTGGATGTCCTTTACCGTCGT	142	NM_017178.1
OPN	GGAGTCCGATGAGGCTATCAA	TCCGACTGCTCAGTGCTCTC	189	M99252.1
BSP	GATAGTTCGGAGGAGGAGGG	CTAACTCCAACTTTCCAGCGT	172	NM_012587
Runx2	ACGTACCCAGGCGTATTTCA	GCTGGATAGTGCATTCGTGG	187	NM_001278483.1
Sox-9	GGGCTCGCGTATGAATCTCC	GCTTGACGTGTGGCTTGTTC	329	XM_001081628.3

To measure attachment and cell viability (3-(4,5-dimethylthiazol-2-yl)-5-(3-carboxymethoxyphenyl)-2-(4-sulfophenyl)-2H-tetrazolium) (MTS) assay (Promega, Madison, WI) was used at days 1, 7, 14, and 28 (n=5). Comparisons were made between TCP, the bone, and cartilage scaffolds.

Chondrogenic and osteogenic gene expression was assessed using reverse transcriptase polymerase chain reaction (RT-PCR). At day 28, RNA was retrieved from each sample, TCP, bone, and cartilage scaffold (n=4) with a Qiagen RNA MiniPrep Kit (Qiagen, Netherlands). RNA concentration was determined using an ND-1000 spectrophotometer (n=4) (Nanodrop, Wilmington, DE), where 2 µg of RNA was transcribed into cDNA using M-MLV Reverse Transcriptase (Promega, Madison, WI) and OligoDT (Invitrogen, Carlsbad, CA) (n=4) accordingly to manufacturer's instructions. The resulting cDNA was combined with Green Mix (Promega, Madison, WI) and primers specific for glyceraldehyde 3-phosphate dehydrogenase (GAPDH), Aggrecan, Sox-9, collagen type I, collagen type II, OPN, BSP, alkaline phosphatase (ALP), BMP-2, and Runt-related transcription factor 2 (Runx-2) are listed in Table 1. GAPDH, as a housekeeping gene, was used to determine relative gene expression. Gel electrophoresis with an 8% agarose gel was used to resolve the DNA with imaging performed with a UVP Photo-Doc Imaging System (UVP, Upland, CA) and all gels were ran with a 1 Kb Plus DNA Ladder (Invitrogen, Grand Island, NY).

2.5 Immunofluorescence Imaging

At day 28, samples were rinsed and then fixed with 4% paraformaldehyde overnight at 4°C. Before incubation in

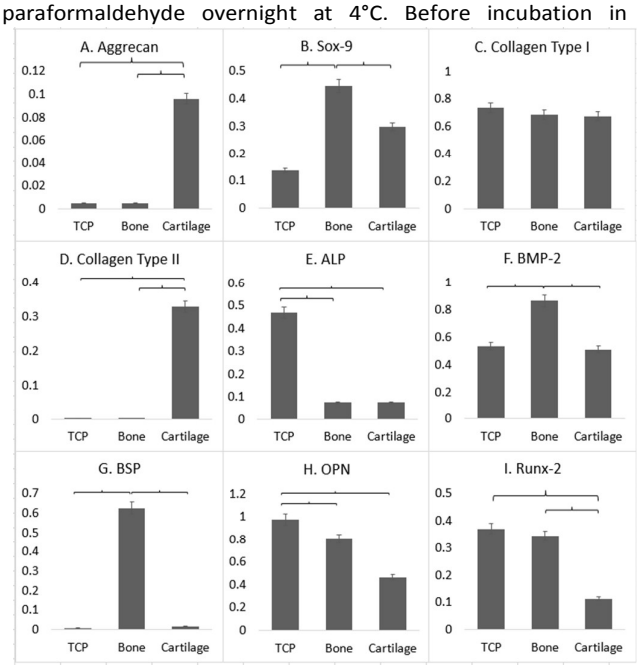

Fig. 5 - Relative expression of chondrogenic and osteogenic genes on TCP control, bone, and cartilage scaffold components: (A) Aggrecan, (B) Sox-9, (C) Collagen type I, (D) Collagen type II, (E) ALP, (F) BMP-2, (G) BSP, (H) OPN, and (I) Runx-2 normalized to GAPDH, brackets indicate the significant differences between each group at p<0.05

primary antibody, all samples were rinsed with tris-buffered saline solution with 1% tween (TBST). Blocking was performed using 5% (w/v) milk in TBST at room temperature for 30 minutes. The spiral scaffolds were then unraveled and sliced

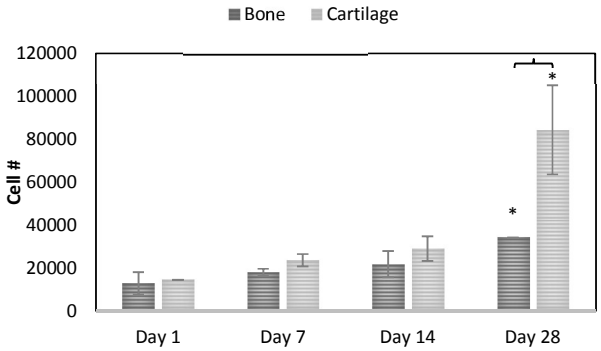

Fig. 3 - MTS Assay data of the bone and cartilage scaffold showing attachment and proliferation of the rat BMSCs, where the bracket shows the signifcant difference between the day 28 samples, an the * indicates significant differences between the different timepoints at p<0.05

into 5 mm lengths so that they could be laid flat on the glass slides. Then they were subsequently incubated in rabbit polyclonal 1:250 anti-aggrecan antibody (ab36861), 1:250 anti-collagen type I (ab34710), 1:250 anti-collagen type II (ab34712), 1:250 anti-osteopontin (ab8448), and 1:250 anti-BMP-2 (ab14933) all from Abcam (Cambridge, MA) in TBST with 5% bovine serum albumin (BSA) overnight at 4°C. Afterwards, they were rinsed 3 times with TBST, then incubated with 1:500 Alexafluor 488 Goat anti-rabbit IgG (Life Technologies, Norwalk, CT) in 5% milk in TBST at room

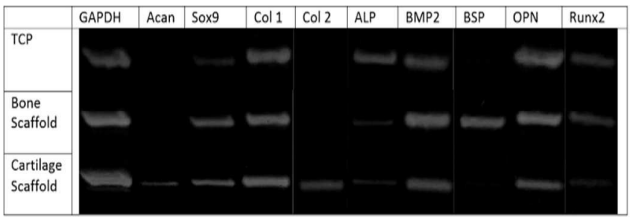

Fig. 4 - RT-PCR bands of the (top) TCP control, (middle) bone scaffold, and (bottom) cartilage scaffold, lane 1: GAPDH, 2: Aggrecan, 3. Sox-9, 4: Collagen type I, 5: Collagen type II, 6: ALP, 7: BMP-2, 8: BSP, 9: OPN, and 10: Runx-2

temperature in the dark for 1.5 hours, then triple rinsed. Nucleic staining and mounting was performed with Fluoroshield with DAPI (Sigma, St. Louis, MO). All images were taken at 20X using a Zeiss Pascal LSM 5 confocal microscope (Germany). Relative secretion of ECM proteins was measured via ImageJ, by splitting the image into the different RGB channels, then plotting intensity of the different colors, where blue would correspond to nucleic material and green, the target protein.

2.6 Statistical Analysis

Statistical analysis of MTS, mechanical testing, relative gene expression of RT-PCR, and relative protein secretion of the immunofluorescence images using ImageJ (n=4) was performed with students T-test *p* values less than 0.05

considered significantly different. All data was reported as a mean ± standard deviation

3. Results

The process of fabricating a biphasic scaffold and its surface topography is presented in Figure 1 and 2. The pull out tests performed at ramp speed of 1.3mm/sec indicated the pull out strength in the range of 10-15 N and two components remained intact.

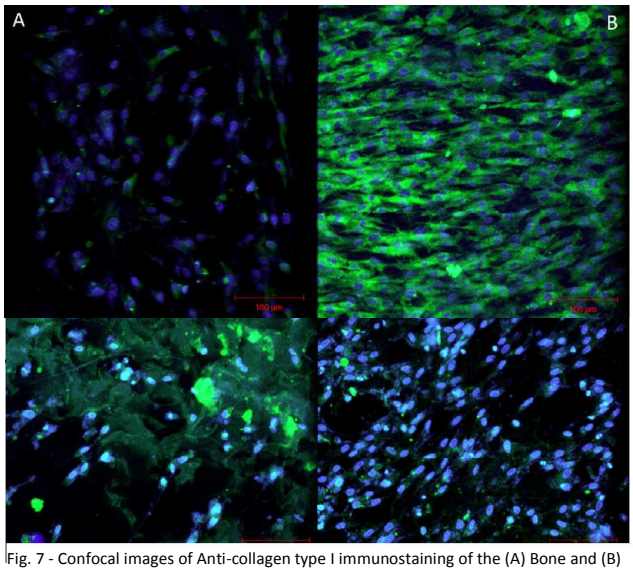

Fig. 7 - Confocal images of Anti-collagen type I immunostaining of the (A) Bone and (B) Cartilage Scaffold

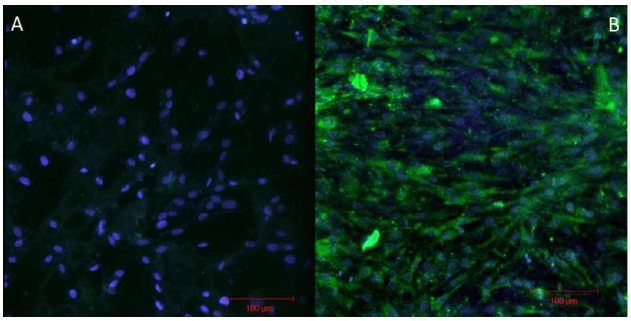

Fig. 8 - Confocal images of Anti-collagen type II immunostaining of the (A) Bone and (B) Cartilage Scaffold

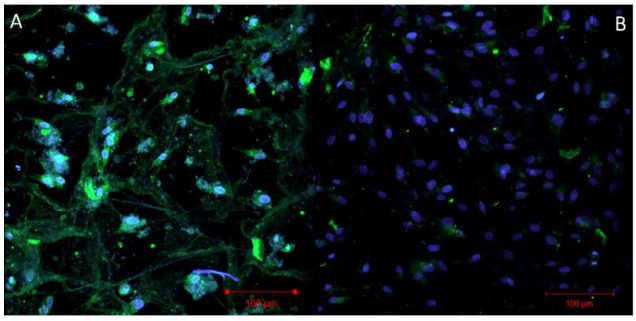

Fig. 9 - Confocal images of Anti-OPN immunostaining of the (A) Bone and (B) Cartilage Scaffold

To determine cytotoxic effects of the scaffold and attachment of the cells, MTS was performed throughout the culture period at days 1, 7, 14, and 28. There was no significant difference in the attachment of the cells at day 1, but by day 28 there was a significant difference ($p<0.05$) in cell viability between the individual bone and cartilage scaffold (Figure 3). In both scaffolds, there was a significant increase in cell number at day 28 when compared to day 1.

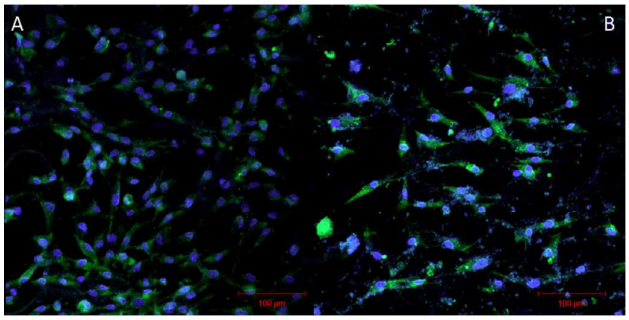

Fig. 10 - Confocal images of Anti-BMP-2 immunostaining of the (A) Bone and (B) Cartilage Scaffold

RT-PCR of each individual scaffold identified increased gene expression of osteogenic and chondrogenic markers compared to that of cells cultured on TCP. Expression of GAPDH was at approximately 334 bp, sox-9 at 329 bp, collagen type I at 280 bp, ALP at 398 bp, BMP-2 at 142 bp, OPN at 189 bp, and Runx-2 at 187 bp as indicated by the bands in the gel from the cells cultured on TCP (Figure 4). In the bone scaffold, there was positive expression for GAPDH, Sox-9, collagen type I, ALP, BMP-2, BSP, OPN, and Runx-2. Gene expression of the cells in cartilage scaffold was similar to that of TCP with the addition of expression of aggrecan at 444 bp and collagen type II at 211 bp.

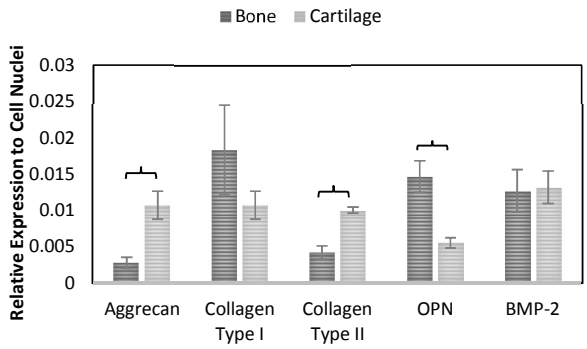

Fig. 11 - The quantitation the target protein of the confocal images relative to the nuclei of the respective images, where brackets indicates significance at $p<0.05$

When quantified with ImageJ densitometry and compared to the respective GAPDH as a normalization marker, the cartilage scaffold demonstrated significant increases in expression of proteins (Figure 5) such as aggrecan (Figure 5A), Sox-9 (Figure 5B) and collagen type II (Figure 5D) when compared to that of TCP. For the bone scaffold, a significant increase in expression of Sox-9, (Figure 5B), BMP-2 (Figure 5F), and BSP (Figure 5G) when compared to that of the cartilage scaffold and TCP. All

samples showed no significant differences in expression of fig. collagen type I (Figure 5C). ALP and OPN expression was significantly higher in the TCP sample when compared to both the bone and cartilage scaffolds (Figure 5E and H). Both TCP sample and the bone scaffold showed a significant increase in Runx-2 expression (Figure 5I).

Protein secretion was visualized through immunofluorescence imaging probing for aggrecan, collagen type I, collagen type II, OPN, and BMP-2. In the images (Figure 6), there is a clear qualitative difference in the amount of aggrecan secreted by the cells, where the cartilage scaffold is seen to secrete much more aggrecan than the bone scaffold. Additionally, the aggrecan is secreted along the alignment of the nanofibers indicating ECM and cellular alignment of the protein. When probed for collagen type I (Figure 7), there is secretion in both scaffolds, but there is significantly more secretion in the bone scaffold, where the collagen type I is expressed not only along the randomly oriented nanofibers, but also in the pores of the PCL scaffold. Clear differences can be seen in the collagen type II immunofluorescence images (Figure 8), where there is an abundance of collagen type II expressed in the cartilage scaffold, compared to the bare minimum of the bone scaffold. Similar to aggrecan secretion, the collagen type II was also aligned to the nanofiber structure. As expected, there is a significant increase in the expression of OPN (Figure 9) in the bone scaffold as compared to the cartilage scaffold, matching the results of the RT-PCR expression. For BMP-2, the imaging (Figure 10) showed BMP-2 secretion in both the bone and cartilage scaffold. From the relative secretion (Figure 11) of the different proteins, significant differences can be seen in the secretion of aggrecan, collagen type II, and OPN. The mechanical testing showed that the retention strength was in the range of 10 to 15 N and that the components remained intact at the heated junction. This strength is equivalent to stature retention strength observed in many surgeries involving grafts and sufficient to withstand ambulatory forces. The failure occurred at the bone side from the tensile tests.

4. Conclusion

The goal of this experiment was to create biomimetic micro-structured spiral PCL scaffolds for the regeneration of bone and cartilage in a biphasic layer to segregate the tissues. Through the novel spiral scaffolds laden with functionalized nanofibers, rat BMSCs differentiated into osteoblast and chondrocyte like cells in the bone and cartilage scaffold, respectively. Additionally, collagen type II fibril alignment was induced with the influence of aligned nanofibers to match that of hyaline cartilage. Observations from the images suggest that cells primarily attach to nanofibers initially and later migrate towards the porous sheet. Nanofibers may provide the most conducive environment for cell attachment. After the cells proliferate towards establishing confluence they migrate towards to available space which is consistent with our previous publications and ongoing studies [23, 28, 30-34].

Due to the lack of cell recognition sites on PCL, it was necessary to functionalize the PCL with materials that promote chondrogenesis. [35] Our results suggest a high degree of alignment of the cells with the nanofibers in the scaffold, indicating the potential for architecturally organized chondrogenesis. In this preliminary *in vitro* experiment, we addressed the ability of the CS and HYA embedded PCL nanofibers to induce rBMSC expression of chondrogenic markers such as aggrecan, collagen type II, and Sox-9. [4, 17, 23, 24, 36] For the bone layer of the PCL with HA scaffold, we assessed expression and secretion of osteogenic markers such as collagen type I, OPN, Sox-9, ALP, BSP and BMP-2. [7, 17, 24, 25] To be a successful osteochondral implant, there needs to be chondrogenesis in the cartilage layer and osteogenesis in the bone layer, and the same stem cells need to be able to differentiate within each zone. Additionally, due to the complex morphology of the collagen type II fibrils in natural cartilage, which provide the mechanical properties of normal articular cartilage, it is imperative to recapitulate that same structure to acquire functional tissue regeneration and organization. The use of HYA in the medium simulates the effect of synovial fluid due to the inclusion of many bioactive factors. [37] Additionally, the use of 1,6 hexanediamine not only increased the active amine binding sites, but also increased hydrophilicity, thereby increasing cell infiltration into the porous substrate structure, which can be seen in the confocal images (Figure 5 - 9). Through the MTS assay, it was determined that the seeding of cells was uniform, as day 1 results showed no significant difference in cell number. But by day 28, it can be seen that there was a significant increase in both the bone and cartilage scaffold, indicating that there was no cytotoxic effect and that there was proliferation throughout the 28 day culture. The lag in proliferation for the cartilage scaffolds from day 1 to day 14 is consistent with previous studies where a lower cell proliferation rate in the beginning is suggestive of early cell differentiation. [38]

To investigate whether the difference in materials can influence the cellular behavior, protein secretion and gene expression were compared among the bone scaffold, cartilage scaffold, and the TCP control. Significant increases in chondrogenic markers of the cartilage scaffold are observed when compared to those of the bone scaffold and the TCP control. The increased expressions of aggrecan and collagen type II are all indicators of hyaline cartilage formation. [38, 39] The confocal images from immunofluorescence corroborate the expression of aggrecan and collagen type II, with the secretion of both proteins. These results are similar to other studies where HYA has been used in either the scaffold or medium to initiate chondrogenesis. [23, 29, 40]

The expression of collagen type I, OPN, ALP, and Runx2 from the cells cultured on the TCP control, indicate hypertrophic cartilage formation, which is a clear difference from the cells in the cartilage scaffold, indicating that HYA in the medium is not enough to drive chondrogenesis alone. [41] Clear indications of osteogenesis in the bone scaffold is shown through the significant expression of BMP-2, BSP, collagen type I, OPN, and Runx2 when compared to the cartilage scaffold. [42] Interestingly, however, the expression of Sox-9 was increased in the bone scaffold, which is usually indicative of

chondrogenesis and in conflict with increased Runx-2, which could be due to the use of HYA in the medium. [43]

Unlike current cell-based approaches or commercially available scaffolds, this novel scaffold has shown a significant increase in collagen type II gene expression showing potential formation of hyaline articular cartilage. In addition and perhaps most importantly, expression follows the alignment of the nanofibers, indicating that the aligned nanofibers can affect the morphology of the cell and the ECM. The CS and HYA can be seen to influence the fate of the cell, as the images show the bone scaffold with HA express minimal aggrecan and type II collagen, though the cell nuclei can be seen from the DAPI staining. Even though all medium used included HYA, the TCP did not show similar gene expression, indicating that the CS and HYA in the nanofibers can influence the cell differentiation. Although BMP-2 is usually associated with osteogenesis, it has been shown that it is expressed in early mesenchymal cells during chondrogenesis. [39] Our RT-PCR and immunofluorescence imaging results corroborate this observation. [44, 45] Minimal expression and secretion of OPN in the cartilage scaffold confirms that the bone formation is mostly confined to the bone scaffold portion, where expression of collagen type I, OPN, and BMP-2 are significantly higher. In hyaline cartilage, a greater ratio of collagen type II to collagen type I usually indicates better tissue formation. The similarity in terms of chondrogenic genes and chondrogenic protein expression was evident on the cartilage component as compared to the bone component. The expression of cartilage like proteins such as aggrecan and collagen type II was significantly higher on cartilage component. However, this trend was not true for all the studies where there were differences in relative gene and corresponding protein expression. Many studies also report such observations where all mRNA does not translate into protein production due to environmental factors [46].

These preliminary results suggest that even when co-cultured together *in vitro,* the different layers of the biphasic osteochondral scaffold should be able to initiate differentiations in the different zones. Due to the limited nature of an *in vitro* study, it is hard to determine how the scaffold will perform *in vivo,* but we believe due to the use of simulated 5% synovial fluid, similar results may be attainable. Additionally, normal synovial fluid in the joint actually has TGF to enhance chondrogenesis and osteogenesis. [29, 47, 48] Future studies will involve placing the bone and cartilage scaffold in the microsphere shell, allowing for measurement of the mechanical properties of the scaffold including ultimate strength and resistance to repetitive stresses in a more physiologic loading environment. The microsphere shell can help resist mechanical compressive stresses and allow for easier implantation into the defect site.

The current study demonstrates that the single structure osteochondral scaffold can differentially induce hyaline-like cartilage tissue in the cartilage layer and bone in the bone layer, with inherent mechanical properties to resist physiological mechanical stresses. Furthermore, the novel feature of the aligned nanofibers has shown the ability to produce tissue that is similar in architecture to natural hyaline cartilage. When combined with another layer of perpendicularly aligned nanofibers on top of the cartilage, the superficial layer of hyaline cartilage can be induced. With the formation of more hyaline-like cartilage, there is the potential of less repeated procedures, decreasing eventual costs, and even an alteration in the unfavorable natural history and progression to osteoarthritis associated with focal cartilage defects.

Acknowledgements

Prof. Yu acknowledges the funding received from the National Science Foundation IIP-1445399 in support of this work. Prof. Kumbar acknowledges the funding from National Science Foundation IIP-1311907, IIP-1355327 and Connecticut Regenerative Medicine Research Fund-15-RMB-UCHC-08.

References

1. L. Lu, X. Zhu, R. G. Valenzuela, B. L. Currier and M. J. Yaszemski, *Clin. Orthop. Relat. Res.*, 2001, **391**, S251.
2. J. E. Browne, A. F. Anderson, R. Arciero, B. Mandelbaum, J. B. Moseley Jr, L. J. Micheli, F. Fu and C. Erggelet, *Clin. Orthop. Relat. Res.*, 2005, **436**, 237.
3. J. B. Moseley Jr, A. F. Anderson, J. E. Browne, B. R. Mandelbaum, L. J. Micheli, F. Fu and C. Erggelet, *Am. J. Sports Med.*, 2010, **38**, 238-246.
4. J. K. Sherwood, S. L. Riley, R. Palazzolo, S. C. Brown, D. C. Monkhouse, M. Coates, L. G. Griffith, L. K. Landeen and A. Ratcliffe, *Biomaterials*, 2002, **23**, 4739-4751.
5. P. Jaiswal, D. Park, R. Carrington, J. Skinner, T. Briggs, A. Flanagan and G. Bentley, *J. Bone Joint Surg. Am.*, 2012, **94**, 131-131.
6. B. M. Cascio and B. Sharma, *Oper. Tech. Sports Med.* , 2008, **16**, 221-224.
7. A. A. Dhollander, K. Liekens, K. F. Almqvist, R. Verdonk, S. Lambrecht, D. Elewaut, G. Verbruggen and P. Verdonk, *Arthroscopy*, 2012, **28**, 225-233.
8. C. Erggelet, M. Endres, K. Neumann, L. Morawietz, J. Ringe, K. Haberstroh, M. Sittinger and C. Kaps, *J. Orthop. Res.*, 2009, **27**, 1353-1360.
9. E. B. Hunziker, *Osteoarthr. Cartil.*, 2002, **10**, 432-463.
10. E. B. Hunziker, *Osteoarthr. Cartil.*, 1999, **7**, 15-28.
11. D. D'lima, S. Hashimoto, P. Chen, C. Colwell and M. Lotz, *Osteoarthr. Cartil.*, 2001, **9**, 712-719.
12. R. Dorotka, U. Windberger, K. Macfelda, U. Bindreiter, C. Toma and S. Nehrer, *Biomaterials*, 2005, **26**, 3617-3629.
13. K. Mithoefer, T. McAdams, R. J. Williams, P. C. Kreuz and B. R. Mandelbaum, *Am. J. Sports Med.*, 2009, **37**, 2053.
14. A. M. Bhosale and J. B. Richardson, *British medical bulletin*, 2008, **87**, 77-95.
15. T. J. Klein, S. C. Rizzi, J. C. Reichert, N. Georgi, J. Malda, W. Schuurman, R. W. Crawford and D. W. Hutmacher, *Macromol. Biosci.*, 2009, **9**, 1049-1058.
16. S. P. Nukavarapu and D. L. Dorcemus, *Biotechnology Advances*, 2013, **31**, 706-721.

17. B. A. Harley, A. K. Lynn, Z. Wissner-Gross, W. Bonfield, I. V. Yannas and L. J. Gibson, *J. Biomed. Mater. Res. A*, 2010, **92**, 1078-1093.
18. J. Wang and X. Yu, *Acta Biomater.*, 2010, **6**, 3004-3012.
19. J. Wang, A. Shah and X. Yu, *Mater. Sci. Eng., C*, 2011, **31**, 50-56.
20. A. Ergun, X. Yu, A. Valdevit, A. Ritter and D. M. Kalyon, *J. Biomed. Mater. Res. A*, 2011.
21. A. Ergun, X. Yu, A. Valdevit, A. Ritter and D. M. Kalyon, *Tissue Eng Part A*, 2012, **18**, 2426-2436.
22. C. Erisken, D. M. Kalyon, H. Wang, C. Örnek-Ballanco and J. Xu, *Tissue Eng Part A*, 2011, **17**, 1239-1252.
23. P. Lee, K. Tran, W. Chang, N. B. Shelke, S. G. Kumbar and X. Yu, *Journal of Biomedical Nanotechnology*, 2014, **10**, 1469-1479.
24. B. A. Harley, A. K. Lynn, Z. Wissner-Gross, W. Bonfield, I. V. Yannas and L. J. Gibson, *J. Biomed. Mater. Res. A*, 2010, **92**, 1066-1077.
25. A. K. Lynn, S. M. Best, R. E. Cameron, B. A. Harley, I. V. Yannas, L. J. Gibson and W. Bonfield, *J. Biomed. Mater. Res. A*, 2009, **92**, 1057-1065.
26. C. M. Valmikinathan, J. Tian, J. Wang and X. Yu, *J Neural Eng*, 2008, **5**, 422.
27. J. Wang, C. M. Valmikinathan, W. Liu, C. T. Laurencin and X. Yu, *J. Biomed. Mater. Res. A*, 2010, **93**, 753-762.
28. X. Zhang, W. Chang, P. Lee, Y. Wang, M. Yang, J. Li, S. G. Kumbar and X. Yu, *PloS one*, 2014, **9**, e85871.
29. A. Hegewald, J. Ringe, J. Bartel, I. Krüger, M. Notter, D. Barnewitz, C. Kaps and M. Sittinger, *Tissue Cell*, 2004, **36**, 431-438.
30. R. James, U. Toti, C. Laurencin and S. Kumbar, in *Biomedical Nanotechnology*, ed. S. J. Hurst, Humana Press, 2011, vol. 726, ch. 16, pp. 243-258.
31. M. Deng, R. James, C. T. Laurencin and S. G. Kumbar, *NanoBioscience, IEEE Transactions on*, 2012, **11**, 3-14.
32. N. A. A. Cheng Y, Valmikinathan C.M, Lee P, Liang D, Yu X, and Kumbar, S.G., *J. Biomed. Nanotech.* , 2013, DOI: 10.1166/jbn.2013.1753.
33. Y. Cheng, D. Ramos, P. Lee, D. Liang, X. Yu and S. G. Kumbar, *Journal of biomedical nanotechnology*, 2014, **10**, 287-298.
34. Y. Cheng, A. A. Nada, C. M. Valmikinathan, P. Lee, D. Liang, X. Yu and S. G. Kumbar, *Journal of Applied Polymer Science*, 2014, **131**.
35. K. Y. Chang, L. H. Hung, I. Chu, C. S. Ko and Y. D. Lee, *Journal of Biomedical Materials Research Part A*, 2010, **92**, 712-723.
36. B. S. Bal, M. N. Rahaman, P. Jayabalan, K. Kuroki, M. K. Cockrell, J. Q. Yao and J. L. Cook, *J. Biomed. Mater. Res. Part B Appl. Biomater*, 2010, **93**, 164-174.
37. J. Chen, C. Wang, S. Lü, J. Wu, X. Guo, C. Duan, L. Dong, Y. Song, J. Zhang and D. Jing, *Cell Tissue Res.*, 2005, **319**, 429-438.
38. A. M. Mackay, S. C. Beck, J. M. Murphy, F. P. Barry, C. O. Chichester and M. F. Pittenger, *Tissue Eng*, 1998, **4**, 415-428.
39. I. Sekiya, J. T. Vuoristo, B. L. Larson and D. J. Prockop, *Proc. Natl. Acad. Sci. U.S.A.*, 2002, **99**, 4397-4402.
40. S. Yamane, N. Iwasaki, T. Majima, T. Funakoshi, T. Masuko, K. Harada, A. Minami, K. Monde and S. Nishimura, *Biomaterials*, 2005, **26**, 611-619.
41. M. Caron, P. Emans, M. Coolsen, L. Voss, D. Surtel, A. Cremers, L. Van Rhijn and T. Welting, *Osteoarthr. Cartil.*, 2012, **20**, 1170-1178.
42. L. Xia, K. Lin, X. Jiang, B. Fang, Y. Xu, J. Liu, D. Zeng, M. Zhang, X. Zhang and J. Chang, *Biomaterials*, 2014, **35**, 8514-8527.
43. C. J. Needham, S. R. Shah, R. L. Dahlin, L. A. Kinard, J. Lam, B. M. Watson, S. Lu, F. K. Kasper and A. G. Mikos, *Acta Biomater.*, 2014, **10**, 4103-4112.
44. I. Sekiya, B. L. Larson, J. T. Vuoristo, R. L. Reger and D. J. Prockop, *Cell Tissue Res.*, 2005, **320**, 269-276.
45. D. Duprez, E. J. de H Bell, M. K. Richardson, C. W. Archer, L. Wolpert, P. M. Brickell and P. H. Francis-West, *Mech. Dev.*, 1996, **57**, 145-157.
46. S. P. Gygi, Y. Rochon, B. R. Franza and R. Aebersold, *Molecular and cellular biology*, 1999, **19**, 1720-1730.
47. K. C. Morrell, W. A. Hodge, D. E. Krebs and R. W. Mann, *Proc. Natl. Acad. Sci. U.S.A.*, 2005, **102**, 14819.
48. R. Okazaki, A. Sakai, Y. Uezono, A. Ootsuyama, N. Kunugita, T. Nakamura and T. Norimura, *J Bone Miner Metab*, 2001, **19**, 228-235.